PHYSICAL REVIEW D

PARTICLES AND FIELDS

THIRD SERIES, VOLUME 35, NUMBER 9 1 MAY 1987

Hadron production in e^+e^- annihilation at $\sqrt{s}=29$ GeV

M. Derrick, E. Fernandez,[a] K. K. Gan,[b] R. Fries,[c] L. Hyman,[d] P. Kooijman, J. S. Loos,[d] B. Musgrave, L. E. Price, J. Schlereth, K. Sugano, J. M. Weiss,[e] and D. E. Wood[f]
Argonne National Laboratory, Argonne, Illinois 60439

G. Baranko,[g] D. Blockus, B. Brabson, M. Daigo,[h] G. E. Forden,[i] S. W. Gray,[j] C. Jung,[b] H. Neal,[k] H. Ogren, D. R. Rust, and M. Valdata-Nappi[l]
Indiana University, Bloomington, Indiana 47405

C. Akerlof, G. Bonvicini, J. Chapman, D. Errede, N. Harnew,[m] P. Kesten,[n] S. Kooijman, D. I. Meyer, D. Nitz, D. Rubin,[j] A. A. Seidl,[o] R. Thun, T. Trinko,[o] and M. Willutzky
University of Michigan, Ann Arbor, Michigan 48109

S. Abachi, P. Baringer, I. Beltrami,[p] B. G. Bylsma, R. De Bonte, D. Koltick, F. J. Loeffler, E. H. Low, U. Mallik,[b] R. L. McIlwain, D. H. Miller, C. R. Ng, P. P. Ong,[q] L. K. Rangan,[o] E. I. Shibata, and R. J. Wilson[r]
Purdue University, West Lafayette, Indiana 47907

B. Cork
Lawrence Berkeley Laboratory, Berkeley, California 94720

L. Keller and J. Va'vra
Stanford Linear Accelerator Center, Stanford, California 94305
(Received 27 October 1986)

Data from the High Resolution Spectrometer at the SLAC storage ring PEP have been used to study the inclusive production of baryons and mesons. Time-of-flight measurements are used to identify the charged hadrons. Neutral hadrons are identified from effective-mass peaks associated with their decay into two charged particles. Cross sections and other inclusive production characteristics are presented for $\pi^{\pm}$, $K^{\pm}$, and K^0 ($\overline{K}^0$) mesons, and for the baryons (antibaryons) p ($\overline{p}$) and Λ ($\overline{\Lambda}$). The ratio of the inclusive cross section to the point cross section for the K^0 and $\overline{K}^0$ mesons is $R(K^0,\overline{K}^0)=6.15\pm0.13\pm0.25$, and for Λ and $\overline{\Lambda}$, $R(\Lambda,\overline{\Lambda})=0.846\pm0.036\pm0.085$. The neutral-hadron differential cross sections are compared with the predictions of the Lund string model.

I. INTRODUCTION

The production cross sections for charged and neutral hadrons in e^+e^- annihilations are important for understanding the fragmentation of quarks and gluons into hadrons. At a center-of-mass energy $\sqrt{s}$ of 29 GeV the dominant reaction is the one-photon annihilation diagram, which has a well-understood initial state within the context of quantum electrodynamics. The final-state quark-antiquark pair, plus any radiated gluons, fragment into observable charged and neutral hadrons.

In this paper, inclusive production cross sections for $\pi^{\pm}$, $K^{\pm}$, K^0, and $\overline{K}^0$, p and $\bar{p}$, and Λ and $\overline{\Lambda}$ produced in e^+e^- annihilations are reported. The measured cross sections for K^0 and $\overline{K}^0$ and Λ and $\overline{\Lambda}$ are compared to the predictions of the Lund fragmentation model.[1] Results for $K^{*0}(890)$ and ρ^0 mesons have already been reported.[2]

These results come from data collected by the High Resolution Spectrometer (HRS) at the SLAC e^+e^- storage ring PEP, which was operated at $\sqrt{s}=29$ GeV. The data used correspond to an integrated luminosity of (185 ± 5) pb^{-1}. The HRS is a general-purpose solenoidal spectrometer. It has been described in detail elsewhere,[3] but briefly, the HRS has a 15-layer central drift chamber plus a 2-layer outer drift chamber for charged-particle tracking, and barrel and end-cap electromagnetic shower calorimeters, all contained in a 1.62-T magnetic field. As discussed in Sec. II, a time-of-flight (TOF) system, which

is part of the barrel calorimeter, was used to identify the charged particles at low momenta (p). As discussed in Sec. IV, neutral hadrons over the full momentum range are identified as V^0 decays, using information from the drift chambers.

II. CHARGED-PARTICLE IDENTIFICATION

Identification of low-momentum ($0.5 \leq p \leq 1.9$ GeV/c) charged particles was achieved by using the time-of-flight (TOF) system, which is an integral part of the electromagnetic shower counters. In the present analysis, only tracks entering the barrel region of the shower-counter system were used. There are 40 barrel modules, 3.05 m long placed parallel to the beam axis with their inner faces at a radius of 1.94 m. This system covers 58% of the total solid angle. As shown in Fig. 1, each module consists of a 3-radiation-length (r.l.) lead-scintillator sandwich, followed by a single layer of 14 proportional wire cells (PWC's), and finally by an 8-r.l. lead-scintillator sandwich. The scintillation light from each sandwich was measured by two Amperex XP2230 phototubes, giving a total of four phototubes and four possible independent measurements of TOF per module. The PWC system is instrumented with current division readout to give a measurement of the z position[4] of a track. The barrel calorimeter system is described in detail in a separate publication.[5]

A bootstrap calibration procedure, using a fast electronic pulser, cosmic-ray data, and $e^+e^- \to e^+e^-$ (Bhabha-scattering) events, kept the TOF system coarsely calibrated during data taking. Fine-tuning was done after complete track reconstruction, using large samples of $e^\pm$ selected from Bhabha-scattering events and of $\mu^\pm$ from $e^+e^- \to \mu^+\mu^-$ events. The measured TOF resolution (σ) is 180 ps for e^+ and e^- tracks from Bhabha-scattering tracks, and about 360 ps for 14.5-GeV/c muon (minimum ionizing) tracks.

For charged-particle identification using TOF, hadronic events were selected according to the following criteria: (a) each event must have five or more good charged-particle tracks; (b) at least one of the tracks must originate from the interaction region, defined by $|z| \leq 0.1$ m and $|r| \leq 0.02$ m, where r is the radial distance from the interaction point in the x-y plane; (c) the scalar sum of the charged-particle track momenta must be greater than 8.7 GeV/c (30% of $\sqrt{s}$); (d) the calorimeter energy must be greater than 1.45 GeV (5% of $\sqrt{s}$). About 78 000 events, with an average of 10.8 reconstructed charged-particle tracks per event, satisfied these criteria.

Tracks originating from the interaction region were examined for TOF identification if they could be associated with a single hit in a barrel module. These charged particles were required to register signals in at least two phototubes when $0.5 \leq p \leq 0.7$ GeV/c or in all four phototubes when $p > 0.7$ GeV/c. In addition, an accepted track had to register a hit in the correct PWC, as determined from the tracking information. Tracks that hit the edge PWC's in any module were excluded in order to avoid tracks with possibly inferior timing information. The TOF analysis could also be confused by tracks accompanied by photons; this contamination was reduced by eliminating the cases where additional PWC hits were registered three or more cells away from the PWC cluster associated with the track. Such confusion was further reduced by requiring consistency between the z positions of the track end as measured by (a) the PWC's, (b) the TOF system, and (c) the drift-chamber tracking projection. These cuts lead to a momentum-dependent weighting factor η_1, which is equal to the ratio of the total number of tracks to the number of selected tracks.[6] An additional factor η_2 is used to correct for the momentum and angle inefficiency in the charged-particle track-reconstruction process. The two weighting factors η_1 and η_2, averaged over the angular range covered by the barrel modules, are given in Table I for each momentum interval. The product of η_1 and η_2 yields the overall correction factor, which ranges from ≈ 22 for the lowest p value to ≈ 6.4 for $p = 1.8$ GeV/c. The TOF of each selected track was calculated as

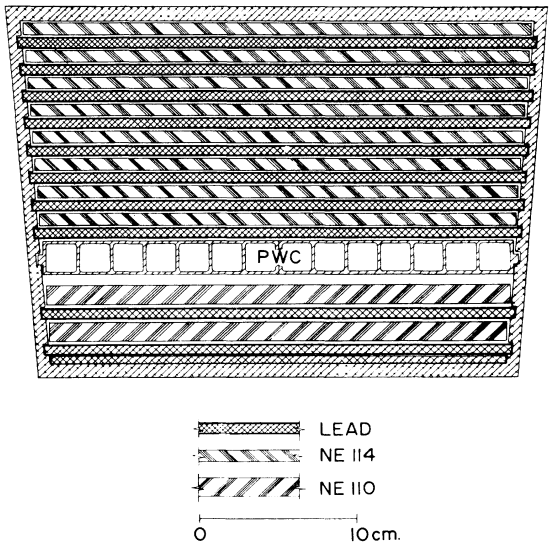

FIG. 1. End view of a barrel calorimeter module.

TABLE I. Weighting factors for the chosen momentum intervals for charged particles identified by time-of-flight techniques. η_1 is the total track count divided by the selected track count; η_2 is the correction for the track-reconstruction efficiency.

Momentum range (GeV/c)	0.5–0.7	0.7–0.9	0.9–1.1	1.1–1.3	1.3–1.5	1.5–1.7	1.7–1.9
η_1	19.33	7.25	5.91	5.58	5.72	5.57	5.70
η_2	1.153	1.142	1.139	1.124	1.129	1.120	1.121
$\eta_1\eta_2$	22.28	8.28	6.73	6.27	6.46	6.24	6.38

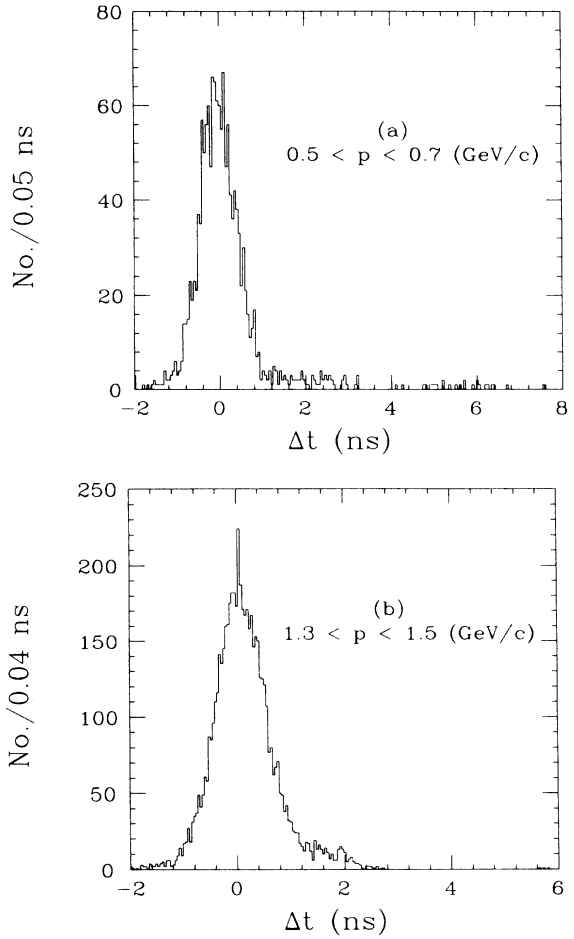

FIG. 2. Difference between the measured time of flight and the expected time of flight for a charged pion for two momentum intervals: (a) $0.5 \leq p \leq 0.7$ GeV/c; (b) $1.3 \leq p \leq 1.5$ GeV/c.

a weighted average of the times of flight measured by the four phototubes. Figure 2 shows the difference between the measured TOF and that expected for a charged pion for two of the momentum intervals considered. For the entire data set the pion peak is well centered at zero with a width corresponding to a σ of about 425 ps. The presence of tracks requiring masses (m) different from that of the pion is clearly seen. $\pi^{\pm}$ and $K^{\pm}$ are separated by $\approx 2\sigma$ at a momentum of 1 GeV/c, and $K^{\pm}$ and p and $\bar{p}$ are separated by $\approx 2\sigma$ at a momentum of 1.6 GeV/c.

III. CHARGED-HADRON RESULTS FROM TIME OF FLIGHT

For each charged-particle track, the measured TOF t and path length l yield the velocity $v=l/t$, and hence $\beta=v/c$. In Fig. 3 a scatterplot of β versus charged-particle momentum is shown. At low momentum $\pi^{\pm}$, $K^{\pm}$, p, and $\bar{p}$ have much different values of β and the charged particles can be identified unambiguously as one of the three particle species. As the momentum increases, the separation in β for the three charged-particle species

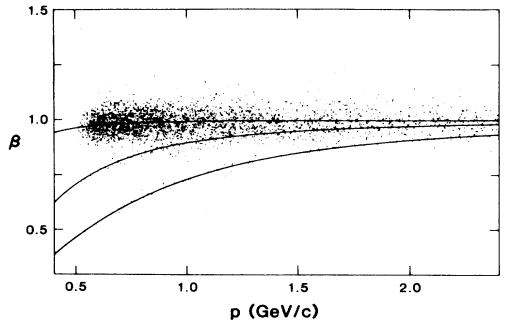

FIG. 3. Scatterplot of $\beta=v/c$ vs momentum for charged particles. The curves are the expected values for $\pi^{\pm}$ (top curve), $K^{\pm}$ (middle curve), and p and $\bar{p}$ (lower curve).

decreases as their velocities approach the speed of light c.

In this analysis each measured value of β has been converted into a value of the mass squared (m^2) of the charged particle by using the relationship

$$m^2=p^2\left[\frac{1-\beta^2}{\beta^2}\right].$$

The m^2 spectra obtained for two of the momentum intervals are displayed in Figs. 4(a) and 4(b). As is evident in Fig. 4(b), the resolution of the TOF system is not good enough to tag unambiguously the identity of each track, especially at the higher momenta. Therefore, a statistical estimate of the particle content in each momentum interval has been used.

Each m^2 spectrum was assumed to be a composite of three Gaussians, centered about the m^2 values of the $\pi^{\pm}$, the $K^{\pm}$, and the p and $\bar{p}$. Using the program MINUIT,[7] the m^2 spectrum was fitted by allowing the normalization of each Gaussian and the width of the Gaussian representing the pion to vary. Since

$$\sigma_{m^2}=\frac{\partial m^2}{\partial t}\sigma_t=\frac{2p^2c^2t}{l^2}\sigma_t$$

and σ_t is essentially independent of the charged-particle species,[8] the widths of the other two Gaussians were determined from the width of the Gaussian representing the $\pi^{\pm}$. The smooth curves in Figs. 4(a) and 4(b) are the results of such fits. There is no statistically significant difference between the spectra of the positive tracks and those of the negative tracks. The area under each Gaussian provides the number of $\pi^{\pm}$, $K^{\pm}$, and p and $\bar{p}$, respectively.

The validity of this procedure was verified by fitting simulated data. Multihadron events were generated by the Lund Monte Carlo program, and the resulting particles were passed through the detector simulation and then processed through the same reconstruction programs. (This overall program is called HRSMC in this paper.) Since the particle identity is known for every track, the number of each particle type generated in a given momentum interval can be compared with the number obtained from TOF fitting. The agreement in all cases was well within the er-

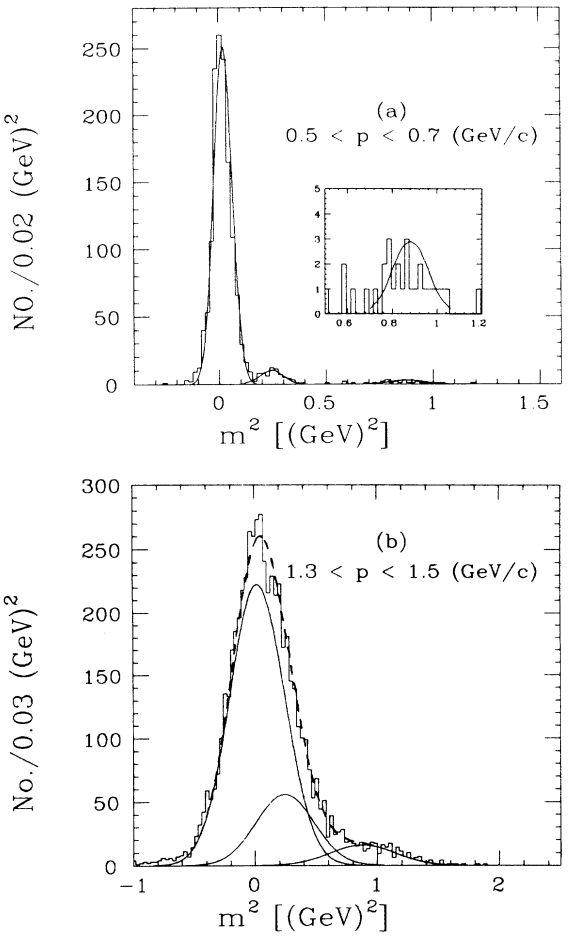

FIG. 4. Mass-squared spectra determined from time-of-flight measurements for two momentum intervals. The three solid curves in each figure correspond to the three Gaussians representing the $\pi^{\pm}$, $K^{\pm}$, and p and $\bar{p}$, fitted as described in the text: (a) $0.5 \leq p \leq 0.7$ GeV/c. The inset shows an expanded view of the fit in the p and $\bar{p}$ m^2 region; (b) $1.3 \leq p \leq 1.5$ GeV/c. The dashed curve is the sum of the three individual Gaussians.

ror estimate of the fit. In particular, the Monte Carlo simulation verified that the track-selection criteria and the correction factors used do not bias the particle fraction results. The same Monte Carlo events are used to estimate and correct for losses from $K^{\pm}$ and $\pi^{\pm}$ decays in flight and for contamination from directly produced $\mu^{\pm}$ and $e^{\pm}$,

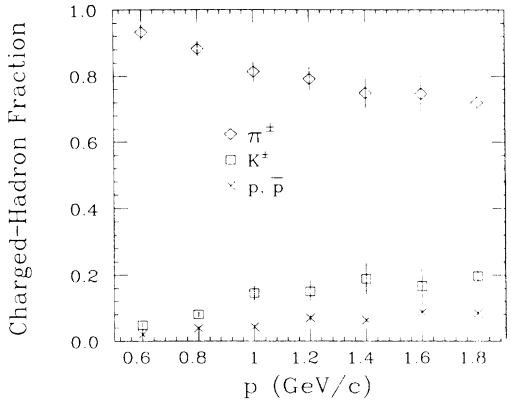

FIG. 5. Charged-particle fractions as a function of momentum.

which are indistinguishable from the $\pi^{\pm}$ in the TOF system.

For the three lowest-momentum bins, this analysis has used (19.6 ± 0.4) pb^{-1} of data taken before the installation of a Cherenkov-counter system.[9] This eliminates the need to make large corrections for the multiple scattering and interactions of p and $\bar{p}$ in the Cherenkov-counter system, which has a thickness of approximately 0.25 r.l. Without the Cherenkov-counter system in place, there is less than 0.03 r.l. of material between the interaction point and the barrel electromagnetic-shower-counter system.

Figure 5 and Table II show the particle fractions as a function of track momentum. With increasing momentum the $\pi^{\pm}$ fraction decreases, and the $K^{\pm}$ and the p and $\bar{p}$ fractions increase. The scaling differential cross sections $(s/\beta)(d\sigma/dz)$ for $\pi^{\pm}$ and $K^{\pm}$, p and $\bar{p}$ are displayed in Fig. 6 and tabulated in Table III as a function of the fractional energy $z = 2E/\sqrt{s}$. The results are compared to the measurements of the Time Projection Chamber[10] (TPC) at the same energy in Fig. 6. For $\pi^{\pm}$ and $K^{\pm}$ the agreement is excellent. For p and $\bar{p}$ the agreement between the TPC and HRS differential cross sections is good, except at $z \approx 0.1$, where two HRS measurements are approximately 3 standard deviations lower than two TPC measurements in the same z region. Systematic errors, which are dominated by uncertainties in the TOF calibration, are included in the HRS error bars. A correction for initial-state radiation[11] has been applied.

TABLE II. Charged-particle fractions. Statistical and systematic errors have been combined.

Momentum range (GeV/c)	$\pi^+ + \pi^-$	$K^+ + K^-$	$p + \bar{p}$
0.5–0.7	0.932±0.025	0.048±0.006	0.020±0.004
0.7–0.9	0.881±0.022	0.080±0.008	0.039±0.005
0.9–1.1	0.813±0.031	0.145±0.022	0.042±0.006
1.1–1.3	0.780±0.035	0.150±0.033	0.070±0.009
1.3–1.5	0.749±0.049	0.188±0.047	0.063±0.004
1.5–1.7	0.745±0.059	0.167±0.056	0.088±0.005
1.7–1.9	0.719±0.092	0.197±0.086	0.084±0.006

TABLE III. Charged-particle invariant cross sections. The units of the invariant cross section $(s/\beta)(d\sigma/dz)$ are μb GeV^2. Statistical and systematic errors have been combined.

Momentum range (GeV/c)	$\pi^+ + \pi^-$ $\langle z \rangle$	$(s/\beta)(d\sigma/dz)$	$K^+ + K^-$ $\langle z \rangle$	$(s/\beta)(d\sigma/dz)$	$p + \bar{p}$ $\langle z \rangle$	$(s/\beta)(d\sigma/dz)$
0.5–0.7	0.042	39.3±1.1	0.054	3.4±0.4	0.077	2.9±0.5
0.7–0.9	0.056	26.8±0.7	0.065	3.4±0.4	0.085	2.8±0.3
0.9–1.1	0.070	18.4±0.8	0.077	4.1±0.6	0.095	1.8±0.3
1.1–1.3	0.083	13.5±0.6	0.089	3.1±0.7	0.105	1.9±0.2
1.3–1.5	0.097	10.5±0.7	0.012	3.0±0.7	0.116	1.3±0.1
1.5–1.7	0.111	8.4±0.7	0.115	2.1±0.7	0.128	1.4±0.1
1.7–1.9	0.125	6.7±0.9	0.129	2.0±0.9	0.140	1.0±0.1

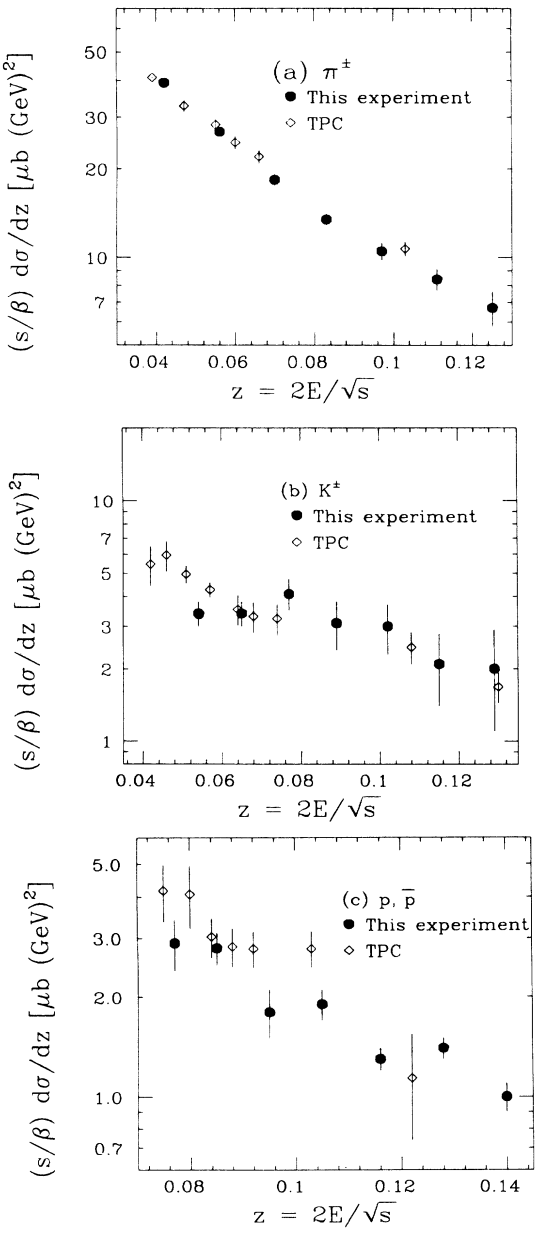

FIG. 6. Scaling differential cross section for (a) $\pi^\pm$; (b) $K^\pm$; (c) p and $\bar{p}$ as a function of the fractional energy $z=2E/\sqrt{s}$. Both statistical and systematic errors are included in the error bars.

IV. IDENTIFICATION OF NEUTRAL HADRONS

The neutral strange particles, the K^0 (and $\bar{K}^0$) and the Λ (and $\bar{\Lambda}$), were identified in the present analysis, using only information from the central and outer drift chambers. The central drift chamber covers 90% of 4π sr with 15 layers of wires located between radii of 0.21 and 1.03 m. The outer chamber covers 60% of 4π with two layers of drift tubes at a mean radius of 1.89 m. The average drift-chamber resolution of 200 μm, combined with the 1.62-T magnetic field, and the small amount of scattering material between the central drift layers and the

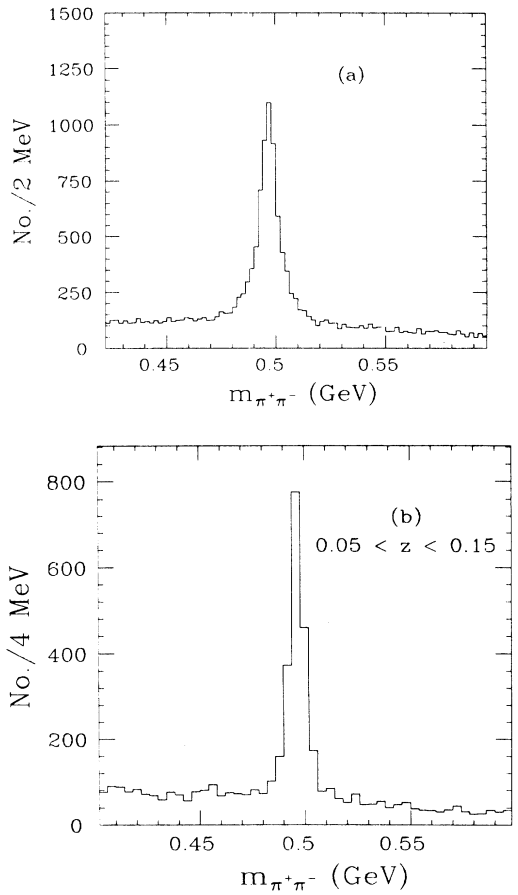

FIG. 7. (a) $\pi^+\pi^-$ effective mass spectrum; (b) $\pi^+\pi^-$ effective mass spectrum for $0.05 < z < 0.15$.

beam interaction point, account for the exceptionally clean and narrow signals from the decays of the K^0 and Λ, as shown in Figs. 7 and 8.

To isolate a sample of charged-particle track pairs from these neutral-hadron decays, conditions were placed upon both individual charged-particle tracks and upon track pairs. The individual track conditions were (1) the χ^2 per degree of freedom from the fitting of the track to the drift chamber hits must be less than 10, (2) the cosine of the production angle of the track relative to the beams is less than 0.9 in magnitude, (3) the momentum component in the x-y plane is greater than 120 MeV/c, (4) the track passes within 0.4 m of the intersection point in the z direction, and within 0.3 m in the x-y plane, (5) at least 50% of the drift-chamber layers traversed by the track were used in the fit, and (6) reconstructed track segments from looping charged-particle tracks are removed.

The algorithm for finding vees began with a systematic pairing of all oppositely charged particle tracks. The two intersection points in the x-y plane were calculated as candidate secondary vertices and each was subject to the following criteria: (1) The distance in the x-y plane from primary to secondary vertex is greater than 5 mm; (2) the difference in the z coordinate between the two tracks at their intersection point is less than 30 mm; (3) the impact parameter of the neutral particle momentum at the primary vertex must be less than 5 mm; (4) the tangent of the angle between the neutral particle's momentum direction and the line connecting the primary and secondary vertices is less than 0.05; (5) the sum of the distances of closest approach to the primary vertex of the two tracks in the x-y plane is greater than 2 mm; (6) the tracks must have no drift-chamber hits between the primary and secondary vertices.

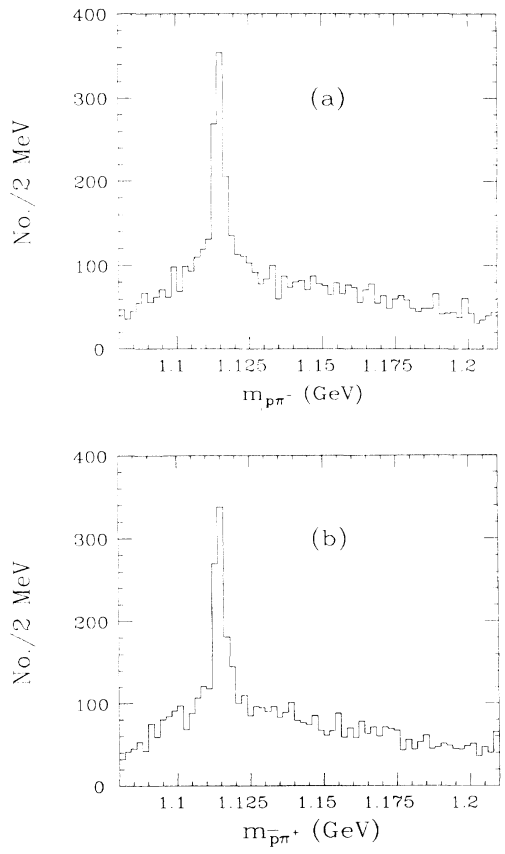

FIG. 8. (a) $p\pi^-$ and (b) $\bar{p}\pi^+$ effective-mass spectra.

The position of the primary vertex was determined by using Bhabha-scattering events from a given run. Twelve tracks from six of these Bhabha events were fit to a common vertex in the x-y plane. The average position of these hybrid Bhabha events for each run gave an intersection-point position which varies slowly with operating conditions of the storage ring. The beam size is roughly described by a σ of 0.5 mm in x and 0.2 mm in y for the distribution of vertex positions obtained.

A fit requiring a common 3-dimensional vertex was done on all pairs of tracks that have at least one x-y intersection that satisfies the above criteria and an effective $\pi^+\pi^-$ ($p\pi^-$) mass within 100 MeV/c^2 of the K^0 (Λ) at that point.

A. K^0 identification

Differences in the decay kinematics and in the lifetimes of the K^0 and Λ require slightly different identification techniques for the two particles. For the K^0, the $\pi^+\pi^-$ spectrum shown in Fig. 7(a) was obtained after the secondary vertex fit and with the addition of further vee conditions appropriate to the K^0. There are 3735 events above the background in the mass interval from 0.492 to 0.502 GeV/c^2. This sample was used for the analysis described in Sec. V of this paper. The additional conditions imposed were (1) a minimum momentum of 0.2 GeV/c for each track is required, (2) each track must pass within 50 mm of the primary vertex in the x-y plane, (3) the required fraction of possible drift-chamber hits on a track is raised from 50% to 70%, (4) the impact parameter limit for the neutral momentum is lowered from 5 to 2 mm, (5) pairs with invariant mass between 1.110 and 1.120 GeV/c^2 when interpreted as a $p\pi^-$ are excluded, and (6) the absolute value of the cosine of the Gottfried-Jackson polar angle must be less than 0.85.

The $\pi^+\pi^-$ mass distribution of Fig. 7(a) was satisfactorily fit by the sum of a linear background and a Breit-Wigner form with the parameters $m(K^0)=(0.4968\pm0.0002)$ GeV/c^2 and full width $\Gamma(K^0)=(9.0\pm0.3)$ MeV/c^2. Figure 7(b) shows the mass distribution for K^0's with fractional energy z in the interval $0.05<z<0.15$, for which the fit parameters are

$$m(K^0)=(0.4966\pm0.0002)\ \text{GeV}/c^2$$

and

$$\Gamma(K^0)=(6.0\pm0.3)\ \text{MeV}/c^2\ .$$

Here also the small and slowly varying background is fit with a linear shape.

Several checks were performed on this K^0 sample, examining, among other things, the distribution in proper time, the production angular distribution, and the decay angular distribution of the K^0. For each distribution, a

background subtraction was made followed by an acceptance correction. The background shape in each case was obtained using pion pairs from the mass intervals (wings) 0.428 to 0.458 GeV/c^2 and 0.538 to 0.568 GeV/c^2, while the K^0 signal was taken from the mass interval 0.492 to 0.502 GeV/c^2. The acceptance corrections were calculated from a complete parallel analysis using HRSMC. These event simulations predict a K^0 signal with a width of (6.0 ± 0.3) MeV/c^2 for the z interval $0.05<z<0.15$, in agreement with that observed.

The proper-time exponential in the corrected data has a slope corresponding to the known K^0 lifetime ($c\tau=0.0267$ m). The production angular distribution is fitted well by the expected $(1+\cos^2\theta)$ distribution, and the cosine of the Gottfried-Jackson polar angle in the rest frame of the K^0 is flat, as expected for the decay of a pseudoscalar particle.

B. Λ selection

Slightly different selection requirements are needed for the Λ baryons due to its longer lifetime ($c\tau=0.0773$ m) and the unequal masses of the two particles in its decay. The additional constraints used for the Λ's were (1) the distance from primary to secondary vertex in the x-y plane is required to be greater than 15 mm, (2) the χ^2 of the constrained fit of the two tracks to the secondary vertex is less than 10.0, (3) the maximum allowed separation in z of the two tracks at the secondary vertex is reduced to 20 mm, (4) the track interpreted as the pion (the track with the smaller momentum of the pair) must miss the primary vertex by at least 2 mm, (5) the impact-parameter limit for the neutral momentum is lowered to 3 mm, which still accepts most Λ's coming from cascade decays, and (6) all pairs with an invariant mass consistent with the K^0 (between 0.488 and 0.508 GeV/c^2) when interpreted as $\pi^+\pi^-$ are removed.

A clean separation of Λ from $\bar{\Lambda}$ can be made using the charge of the higher-momentum decay particle. Kinematics dictates that the proton carry most of the momentum in the laboratory frame for a Λ with laboratory momentum greater than 300 MeV/c, allowing us to make a unique $p\pi^-$ ($\bar{p}\pi^+$) mass assignment to the two tracks. The $p\pi^-$ and $\bar{p}\pi^+$ mass spectra are shown in Fig. 8. A Breit-Wigner form on a second-order polynomial background was fit to the peak region. The Breit-Wigner parameters for these fits are

$$m(\Lambda)=(1.1156\pm0.0001)\ \text{GeV}/c^2\ ,$$
$$\Gamma(\Lambda)=(5.01\pm0.38)\ \text{MeV}/c^2\ ,$$
$$m(\bar{\Lambda})=(1.1156\pm0.0001)\ \text{GeV}/c^2\ ,$$
$$\Gamma(\bar{\Lambda})=(4.79\pm0.38)\ \text{MeV}/c^2\ .$$

The widths of the peaks agree well with those from the HRSMC events. The areas under the Breit-Wigner curves correspond to (970 ± 50) Λ and (890 ± 40) $\bar{\Lambda}$ events, showing equal numbers of the Λ and its antiparticle. Other fits using different functional forms for the background shape were tried and consistent results were obtained.

Because the Λ mass is near the proton-pion threshold, a background subtraction technique different from the one used for the K^0's was needed. For the Λ analysis, a background distribution was calculated from normal events where a simple reversal of the direction of all the negative tracks was performed. This track mixing removed any positive-negative track correlations, and hence any true vee pairs. A completely parallel analysis of Monte Carlo events, including track mixing, was done to give the appropriate acceptance corrections. The overall acceptance for the Λ's is 5.3%, integrated over all momenta and including the $p\pi^-$ branching fraction of 64.2%. The corrected proper-time distribution gave a slope which was in good agreement with the known Λ lifetime.

V. NEUTRAL-HADRON RESULTS

The scaling differential cross sections $(s/\beta)(d\sigma/dz)$ for the K^0 and $\bar{K}^0$ are given in Table IV. These results are compared with the predictions of the Lund string model[12] in Fig. 9(a). The agreement is reasonable. Figures 9(b) and 9(c) show data from other e^+e^- experiments in the same energy range[13–16] together with the same Lund curve.

In Fig. 10 the scaling cross sections for the charged and neutral kaons are shown together with the Lund prediction. For $z>0.07$ the charged and neutral-scaling cross sections are in excellent agreement with each other and with the Lund prediction. For $z<0.07$ the charged-kaon scaling cross section is lower than that for neutral kaons by a factor of ≈2 at $z\approx0.05$ with the Lund prediction falling in between the two.

After correction for the unobserved z regions, a K^0 and $\bar{K}^0$ inclusive cross section of $\sigma(K^0,\bar{K}^0)=667\pm14\pm25$ pb is measured. The first error is statistical while the second is systematic and reflects the uncertainties in the acceptance and the measured luminosity. The branching ratio of $K^0\to\pi^+\pi^-$ was taken to be 34.3%. This cross section corresponds to an R value $\sigma(K^0,\bar{K}^0)/\sigma(\mu^+\mu^-)$, corrected for the effects of initial-state radiation,[10] of $R(K^0,\bar{K}^0)$

TABLE IV. K^0 and $\bar{K}^0$ invariant cross section. The first error is statistical. The second error is systematic and reflects the uncertainties in the acceptance, the correction for initial-state radiation, and the measured luminosity.

z	$(s/\beta)(d\sigma/dz)$[μb(GeV)^2]
0.0343–0.060	8.37 ±0.50±0.68
0.06–0.10	3.97 ±0.13±0.20
0.10–0.14	1.90 ±0.07±0.10
0.14–0.18	1.20 ±0.05±0.07
0.18–0.22	0.781±0.050±0.058
0.22–0.26	0.626±0.044±0.055
0.26–0.30	0.532±0.046±0.056
0.30–0.40	0.289±0.021±0.026
0.40–0.50	0.130±0.013±0.018
0.50–0.60	0.046±0.012±0.010
0.60–0.70	0.013±0.008±0.005
0.70–0.80	0.000±0.003±0.001
0.80–1.00	0.003±0.003±0.002

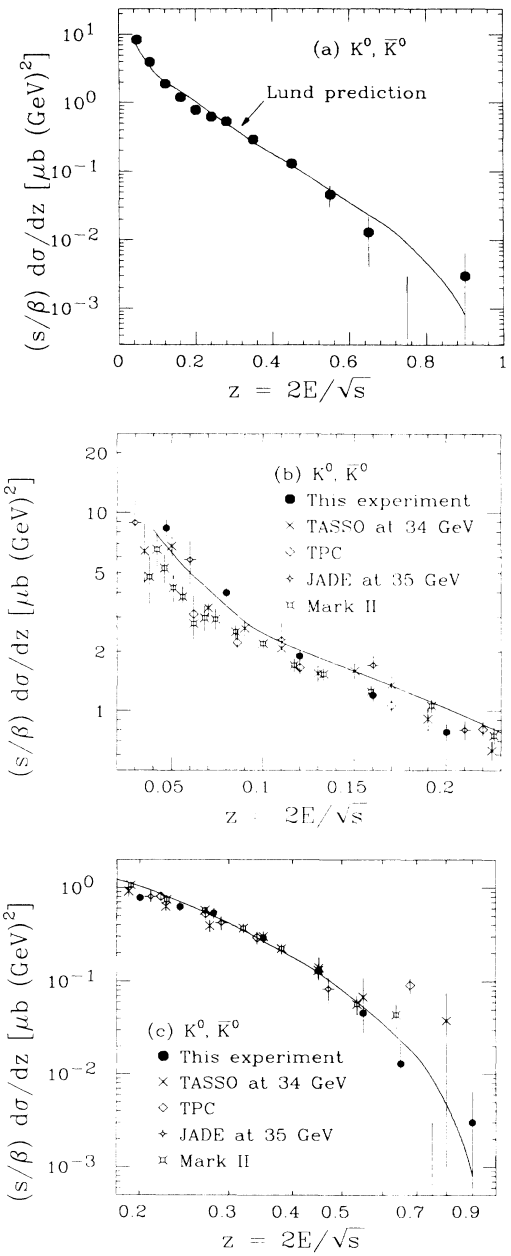

FIG. 9. (a) Comparison of the HRS scaling cross section for K^0 and $\overline{K}^0$ with the prediction of the Lund string model. Both statistical and systematic errors are included in the error bars; (b) scaling cross sections for K^0 and $\overline{K}^0$ from HRS and other e^+e^- experiments in the same energy range at low z; (c) scaling cross sections for K^0 and $\overline{K}^0$ from HRS and other e^+e^- experiments in the same energy range for $z>0.18$.

$=6.15\pm0.13\pm0.25$. Using the MAC measurement[17] of $R(\text{hadronic})=3.90\pm0.04\pm0.12$, the number of K^0 and $\overline{K}^0$ per hadronic event is

$$\langle N(K^0,\overline{K}^0)\rangle = R(K^0,\overline{K}^0)/R(\text{hadronic})$$
$$= 1.58\pm0.03\pm0.08\ .$$

This can be compared with other recent measurements;[18]

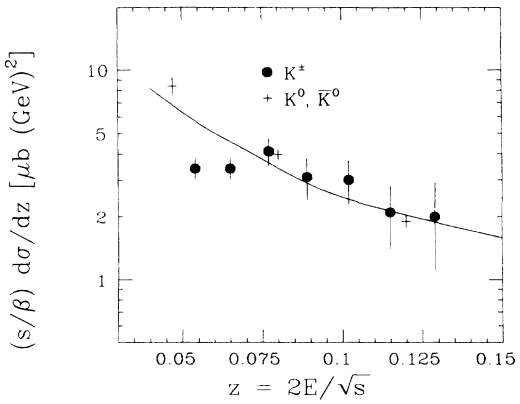

FIG. 10. Scaling cross sections for charged and neutral kaons. The solid curve is the prediction from the Lund model.

TASSO reports 1.48 ± 0.05 K^0's per event, and JADE measures $1.49\pm0.22\pm0.15$ K^0's per event, both at 34 GeV; the TPC observes $1.22\pm0.03\pm0.15$ K^0's per event at 29 GeV; Mark II reports $1.27\pm0.03\pm0.15$.

Figure 11 and Table V show the scaling cross section for Λ and $\overline{\Lambda}$ as a function of the fractional energy. Comparison with other e^+e^- experiments[19,20] in Fig. 11 shows good agreement.

The radiatively corrected R value for Λ and $\overline{\Lambda}$ in the fractional energy interval $0.1<z<0.8$ is $0.669\pm0.029\pm0.051$. Using the Lund-model predictions to correct for unmeasured energy regions gives $R(\Lambda,\overline{\Lambda})=0.846\pm0.036\pm0.085$, which corresponds to $\langle N(\Lambda,\overline{\Lambda})\rangle = 0.217\pm0.009\pm0.022$ per hadronic event.

These R-value measurements for the K^0 and Λ are shown in Fig. 12, together with results from other e^+e^- experiments.[21] The curves are drawn to show logarithmic rises with $W=\sqrt{s}$ and are normalized to the HRS values at 29 GeV. The K^0 and $\overline{K}^0$ R values from all experiments taken together support a logarithmic rise with W. However, the Λ data show a steeper increase with W.

Fourteen events containing both a Λ and a $\overline{\Lambda}$ were observed. The estimated background to this signal, obtained

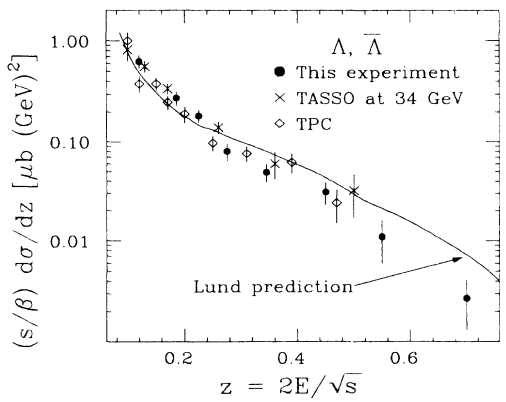

FIG. 11. Scaling cross sections for Λ and $\overline{\Lambda}$ as a function of the fractional energy. Both statistical and systematic errors are included in the error bars.

TABLE V. Λ and $\bar{\Lambda}$ invariant cross section. The first error is statistical. The second error is systematic and reflects the uncertainties in the acceptance, the correction for initial-state radiation, and the measured luminosity.

z	$(s/\beta)(d\sigma/dz)[\mu b(\text{GeV})^2]$
0.10—0.15	0.628 ±0.051±0.077
0.15—0.20	0.275 ±0.023±0.037
0.20—0.25	0.183 ±0.017±0.021
0.25—0.30	0.080 ±0.012±0.010
0.30—0.40	0.049 ±0.007±0.008
0.40—0.50	0.031 ±0.006±0.006
0.50—0.60	0.011 ±0.004±0.003
0.60—0.80	0.0027±0.0012±0.0007

from the track-mixed events, is (2.6 ± 1.9) events. An alternative background estimation found no events where a Λ ($\bar{\Lambda}$) in the peak region of the mass plot is paired with a $\bar{\Lambda}$ (Λ) in the wings. Background pairings were observed to arise primarily from tracks which were duplicated in the track-finding process, giving Λ and $\bar{\Lambda}$ which were similar in mass, rapidity, and laboratory angle. The 14 events, with this background estimation, correspond to $\langle N(\Lambda\bar{\Lambda})\rangle=(0.051\pm0.017\pm0.011)$ pairs per hadronic event. This number has bearing on the Lund diquark parameters, as will be discussed in the following section. Comparing this number with $\langle N(\Lambda,\bar{\Lambda})\rangle=0.217$, we see that the strangeness and the baryon number of the Λ are compensated by something other than a $\bar{\Lambda}$ (or an antibaryon which decays to a $\bar{\Lambda}$) roughly half the time.

In Figs. 13(a)—13(c) the angular separations, rapidity differences, and transverse-momentum correlations of the 14 ($\Lambda\bar{\Lambda}$) pairs in the laboratory frame are presented. While the $\cos\theta$ and Δy distributions are consistent with models featuring local baryon-number compensation, the lack of correlation in transverse momentum favors a picture where the baryon and antibaryon are not always neighboring in rank. The Lund "popcorn" model,[22] with the default parameter

$$P(BM\bar{B})/[P(B\bar{B})+P(BM\bar{B})]=0.5\ ,$$

gives reasonable agreement with the data. However, lack of statistics prevents any meaningful quantitative measure of this parameter or, in general, of the importance of

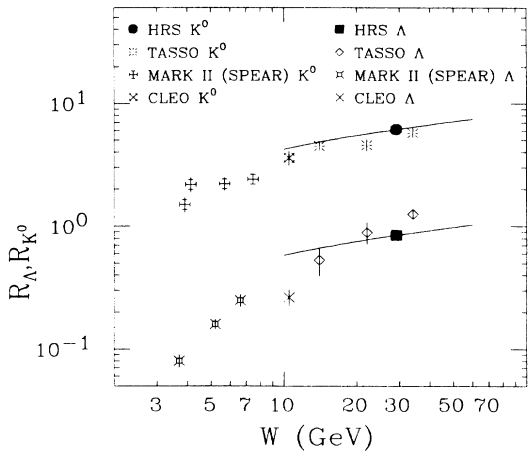

FIG. 12. R-value measurements for inclusive K^0 and Λ production from e^+e^- annihilations vs center-of-mass energy $W=\sqrt{s}$. The curves represent logarithmic rises with W and are normalized to the HRS values at 29 GeV.

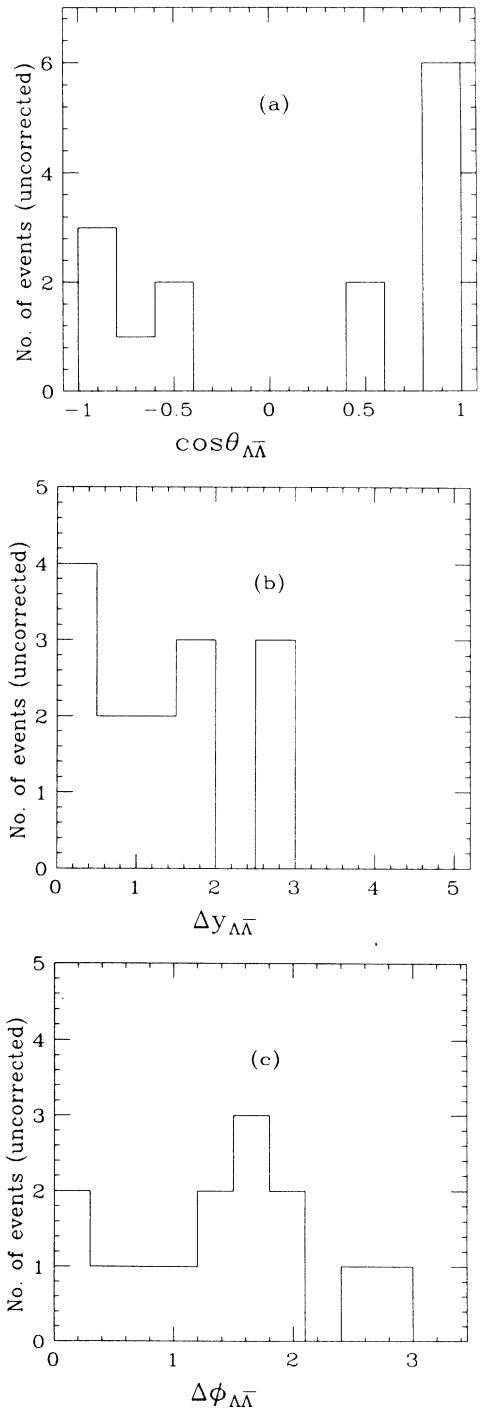

FIG. 13. (a) Angular separations; (b) rapidity differences; and (c) transverse-momentum correlations of the 14 $\Lambda\bar{\Lambda}$ pairs in the laboratory frame.

TABLE VI. Lund-model parameters.

Parameter	TPC	HRS	Lund
$P(qq)/P(q)$	0.078±0.005	· · ·	0.10
$P(s)/P(u)$	0.25 ±0.016	0.34±0.03	0.30
$[P(us)/P(ud)]/[P(s)/P(d)]$	0.73 ±0.09	0.87±0.06	0.40
$P(V)/P(V+P)(u,d)$	0.32 ±0.05	0.54±0.06	0.50
$P(V)/P(V+P)(s)$	0.35 ±0.03	0.66±0.08	0.60
$P(V)/P(V+P)(c,b)$	· · ·	$1.0^{+0.2}_{-0.3}$	0.75

mechanisms giving a non-neighboring baryon and antibaryon. Also, as Ekelin and Fredriksson[23] point out, the absence of spin forces in a system of spin-zero diquark and antidiquark can dilute the transverse-momentum correlations even if baryon and antibaryon are always neighboring. Finally, we also note that nine pairs of the type $\Lambda\Lambda$ or $\bar{\Lambda}\bar{\Lambda}$, were observed with an estimated background of (7.8±3.0) pairs.

VI. COMPARISON OF THE NEUTRAL-HADRON RESULTS WITH THE LUND MODEL

In contrast with the charged-hadron differential cross sections presented in this paper, the K^0 and $\bar{K}^0$ and Λ and $\bar{\Lambda}$ differential cross sections are measured over a large momentum range. It is of particular interest to compare these latter distributions with the predictions of existing Monte Carlo models such as the Lund string model. In this context we discuss the Lund-model parameters given in Table VI which shows the default parameter values of Lund version 5.3, the values obtained by the TPC Collaboration,[24] and the values that best reproduce the cross sections measured by the HRS.

These Lund parameters dictate the relative probabilities for the sea production of strange quarks (s) versus light quarks (u and d) and diquarks (qq) versus quarks (q), and for forming vector (V) versus pseudoscalar (P) mesons. Our values for $P(s)/P(u)$, $P(V)/P(V+P)(u,d)$, $P(V)/P(V+P)(s)$, and $P(V)/P(V+P)(c,b)$ come from the analysis of K^{*0} and ρ^0 and D cross sections,[25,26] while the $[P(us)/P(ud)]/[P(s)/P(d)]$ value is derived from the Λ and $\bar{\Lambda}$ cross sections presented in this paper. We have used the TPC value for $P(qq)/P(q)$ as determined from their proton cross section.

To reproduce the z distribution of the Λ well requires a change to the branching ratios for charmed baryons decaying to Λ in Lund version 5.3. Using the default method of the Monte Carlo program, the inclusive branching ratio for $\Lambda_c \to \Lambda X$ is 50%, and some 20% of all Λ baryons come from this source. Using instead the best experimental measurement of this branching ratio (Ref. 27) $B(\Lambda_c \to \Lambda X) = 23 \pm 10\%$ the χ^2 of the fit to the z distribution improves dramatically, and the fitted value of $[P(us)/P(ud)]/[P(s)/P(d)]$ changes considerably. Without adjusting the charmed-baryon decays, we obtain

$$[P(us)/P(ud)]/[P(s)/P(d)] = 0.23 \pm 0.05 ,$$

whereas with the adjustment the fitted value is

$$[P(us)/P(ud)]/[P(s)/P(d)] = 0.87 \pm 0.06 .$$

The correlations between the value of $[P(us)/P(ud)]/[P(s)/P(d)]$ and other Lund-model parameters, and with the charmed-baryon branching ratios, were not taken into account in calculating the quoted errors.[28] Varying the charmed-baryon branching ratio by ±10% about the value 23% does not change the result. We also note that the Lund prediction for $\langle N(\Lambda\bar{\Lambda}) \rangle$ is relatively insensitive to $B(\Lambda_c \to \Lambda X)$, and we can use our measured value to independently determine $[P(us)/P(ud)]/[P(s)/P(d)]$. The value so obtained is 0.87±0.50, in agreement with our value from the fit to the inclusive Λ z distribution.

The z distribution of the K^0's is less sensitive to variations among the Lund parameters and is well reproduced by any of three sets of parameters in Table VI. Similarly, the charged-hadron cross sections, in their limited momentum range, can be easily fitted. The agreement of the $K^{\pm}$ and K^0 cross sections in the region of overlap allows the Lund model to reproduce both production rates with its one strangeness suppression parameter. It is also significant that the fragmentation function used in the Lund model succeeds in describing the scaling cross sections of each of the particles presented here.

VII. SUMMARY AND CONCLUSIONS

The inclusive production cross sections have been measured for $\pi^{\pm}$, $K^{\pm}$, p, and $\bar{p}$, K^0 and $\bar{K}^0$, and Λ and $\bar{\Lambda}$ in e^+e^- annihilations at $\sqrt{s} = 29$ GeV. A time-of-flight system was used to identify the charged particles in the momentum interval $0.5 < p < 1.9$ GeV/c. The neutral hadrons were identified as V^0 decays, using information from a drift-chamber system, over the full momentum range. In general, the scaling differential cross sections $(s/\beta)(d\sigma/dz)$ are in good agreement with those of other e^+e^- annihilation experiments. The Lund string model reproduces the cross sections for the charged hadrons and the K^0 and $\bar{K}^0$ quite well, but an adjustment of some of the Lund-model parameters away from the default values and those obtained by TPC is required to fit the Λ and $\bar{\Lambda}$ cross sections over the full momentum range.

The data we have presented in this paper, and the ability of a model such as the Lund to fit the data, provide some insight into the process of quark fragmentation into hadrons. These observations and these models provide a basis for further and more detailed attempts to understand this complex process, and to seek its roots in the theory of the strong interactions.

ACKNOWLEDGMENTS

This work was supported in part by the U.S. Department of Energy under Contract Nos. W-31-109-ENG-38 (Argonne National Laboratory), DE-AC02-84ER40125 (Indiana University), DE-AC02-76ER01112 (University of Michigan), DE-AC02-76ER01428 (Purdue University), DE-AC03-76SF00098 (Lawrence Berkeley Laboratory), and DE-AC03-76SF00515 (Stanford Linear Accelerator Center). The experiment was made possible by the support provided by the PEP staff and the technical staffs of the collaborating institutions. This paper is based, in part, on the Ph.D. theses of Ong[29] and Baringer.[30]

---

[a]Present address: University of Barcelona, Bellaterra, Spain.
[b]Present address: Stanford Linear Accelerator Center, Stanford, CA 94305.
[c]Present address: Ecole Polytechnique, F-91128 Palaiseau, France.
[d]Present address: AT&T Bell Laboratories, Naperville, IL 60566.
[e]Present address: SRI International, Menlo Park, CA 94025.
[f]Present address: ESL, Sunnyvale, CA 94088.
[g]Present address: University of Colorado, Boulder, CO 80309.
[h]Visitor from Wakayama Medical College, Japan.
[i]Present address: Rutherford Appleton Laboratory, Chilton, U.K.
[j]Present address: Laboratory of Nuclear Studies, Cornell University, Ithaca, NY 14853.
[k]Permanent address: SUNY, Stony Brook, NY 11794.
[l]Permanent address: INFN, Pisa, Italy.
[m]Present address: University of Oxford, Oxford, U.K.
[n]Present address: Brandeis University, Waltham, MA 02254.
[o]Present address: Lockheed Missiles and Space Co., Sunnyvale, CA 94086.
[p]Present address: CERN, CH1211 Geneva 23, Switzerland.
[q]Present address: Electronic Data Systems of Canada, Oshawa, Canada.
[r]Present address: Boston University, Boston, MA 02215.

[1]B. Andersson, G. Gustafson, and T. Sjostrand, Phys. Rep. **97**, 33 (1983). Version 5.3 of the Lund Monte Carlo model has been used.
[2]M. Derrick *et al.*, Phys. Lett. **158B**, 519 (1985).
[3]D. Bender *et al.*, Phys. Rev. D **30**, 515 (1984).
[4]A right-handed spatial coordinate system is used. In it the z axis points along the direction of the positron beam (which also coincides with the direction of the axial magnetic field), the y axis points vertically upward, and the x axis points radially inward in the plane of the PEP ring.
[5]J. S. Loos *et al.*, Nucl. Instrum. Methods **A249**, 185 (1986).
[6]η_1 is the product of weights that correct for (a) limited solid-angle coverage of the barrel calorimeter (≈ 2.1), (b) the requirements that the track is the only one in a module, that it does not pass into adjacent modules, and that the PWC's and the appropriate number of phototubes have information (≈ 2.9), and (c) the requirement that the three z-position measurements are consistent (≈ 2.1). Only the subset of tracks with transverse momentum greater than 0.5 GeV/c reach the barrel modules, because of the magnetic field, so that η_1 is especially large for $0.5 < p < 0.7$ GeV/c.
[7]F. James and M. Roos, 1978 CERN Computer Centre Report No. D 506 (unpublished).
[8]Different species of charge particles with the same momentum will lose different amounts of energy in the scintillator and therefore generate different amounts of light. Since the TOF resolution is better for large amplitude signals, there is, in principle, a slight difference in TOF resolution for the different particle species.
[9]N. Harnew and D. Meyer, Nucl. Instrum. Methods **186**, 513 (1981).
[10]H. Aihara *et al.*, Phys. Rev. Lett. **52**, 577 (1984).
[11]Lund-model Monte Carlo events which survive both the trigger and event selection have an average center-of-mass energy $\sqrt{s}=(28.3\pm0.2)$ GeV. Thus, scaling cross sections are calculated with $s=(801\pm11)$ GeV^2. $\sigma(\mu^+\mu^-)=(108.5\pm1.5)$ pb has been used in the R-value calculations.
[12]See Sec. VI for a discussion of the Lund parameters used in this analysis.
[13]R. Brandelik *et al.*, Phys. Lett. **94B**, 91 (1980).
[14]W. Bartel *et al.*, Z. Phys. C **20**, 187 (1983).
[15]H. Aihara *et al.*, Phys. Rev. Lett. **53**, 2378 (1984).
[16]H. Shellman *et al.*, Phys. Rev. D **31**, 3013 (1985).
[17]E. Fernandez *et al.*, Phys. Rev. D **31**, 1537 (1985).
[18]Ch. Berger *et al.*, Phys. Lett. **104B**, 79 (1981); and Refs. 13–16.
[19]M. Althoff *et al.*, Z. Phys. C **27**, 27 (1985).
[20]H. Aihara *et al.*, Phys. Rev. Lett. **54**, 274 (1985).
[21]S. Behrends *et al.*, Phys. Rev. D **31**, 2161 (1985); M. Piccolo *et al.*, Phys. Rev. Lett. **39**, 1503 (1977); V. Luth *et al.*, Phys. Lett. **70B**, 120 (1977); and Ref. 19.
[22]B. Andersson, G. Gustafson, and T. Sjostrand, Phys. Scr. **32**, 544 (1985).
[23]S. Ekelin and S. Fredriksson, Phys. Rev. Lett. **56**, 2428 (1986).
[24]H. Yamamoto, in *QCD and Beyond,* proceedings of the Twentieth Rencontre de Moriond, 1985, edited by J. Tran Thanh Van (Editions Frontières, Gif-sur-Yvette, France, 1985), p. 91.
[25]M. Derrick *et al.*, Phys. Lett. **158B**, 519 (1985).
[26]M. Derrick *et al.*, Phys. Rev. Lett. **53**, 1971 (1984).
[27]K. Abe *et al.*, Phys. Rev. D **33**, 1 (1986).
[28]Analysis based on 256 pb^{-1} of data gives a value for $[P(us)/P(ud)]/[P(s)/P(d)]$ in good agreement with that presented here. See P. Baringer *et al.*, Phys. Rev. Lett. **56**, 1346 (1986).
[29]P. P. Ong, Ph.D. thesis, Purdue University, 1983, Report No. PU-83-505.
[30]P. Baringer, Ph.D. thesis, Indiana University, 1985, Report No. IUHEE 61.